Check for updates

Cerium(IV) oxide:silver/graphene oxide (CeO$_2$:Ag/GO) nanoparticles modulate gene expression and inhibit colorectal cancer cell growth: a pathway-centric therapeutic approach

Omid Reza Tamtaji[1†], Amirreza Ostadian[2†], Mina Homayoonfal[3†], Majid Nejati[4], Maryam Mahjoubin-Tehran[5,6], Fatemeh Nabavizadeh[7], Elaheh Ghelichi[8], Bahareh Mohammadzadeh[9], Merat Karimi[9*], Neda Rahimian[10,11*] and Hamed Mirzaei[3*]

†Omid Reza Tamtaji, Amirreza Ostadian, and Mina Homayoonfal have contributed equally to this work.

*Correspondence:
merat.karimi123@gmail.com; Rahimian.n@iums.ac.ir; mirzaei-h@kaums.ac.ir; h.mirzaei2002@gmail.com

³ Research Center for Biochemistry and Nutrition in Metabolic Diseases, Institute for Basic Sciences, Kashan University of Medical Sciences, Kashan, Iran
⁹ Institute of Nanoscience and Nanotechnology, University of Kashan, Kashan, Iran
¹¹ Endocrine Research Center, Institute of Endocrinology and Metabolism, Iran University of Medical Sciences (IUMS), Tehran, Iran
Full list of author information is available at the end of the article

Abstract

Colorectal cancer (CRC) represents a substantial global health burden, necessitating advancements in diagnostic and therapeutic modalities. This study aimed to investigate the potential of CeO$_2$/GO nanoparticles (NPs) in managing CRC and to compare their efficacy with Ag-doped CeO$_2$ (CeO$_2$:Ag) NPs. The synthesis of cerium oxide (CeO$_2$) and graphene oxide (GO) was meticulously performed, followed by a comprehensive evaluation of NPs' toxicity and their impact on apoptosis-related genes in CRC cells. Characterization techniques, including XRD, EDX, SEM, TEM, FT-IR, and DLS, validated the successful synthesis and unique properties of CeO$_2$:Ag/GO NPs. XRD confirmed the CeO$_2$ and GO structures, while EDX analysis confirmed high purity in the synthesized NPs and uniform element distribution in CeO2/GO NPs. SEM and TEM micrographs illustrated CeO$_2$ NPs attached to graphene sheets, showcasing reduced size post-attachment. FT-IR revealed characteristic peaks for CeO$_2$ and GO, confirming their composite structure. DLS showed an average NP size of 20 nm in solution. Notably, MTT assays demonstrated that CeO$_2$:Ag/GO NPs exhibited enhanced cytotoxicity against CRC cells (C-26 cell line) compared to CeO$_2$:Ag NPs, with higher doses showing heightened efficacy. CeO$_2$:Ag/GO NPs induced stronger growth inhibition and apoptosis in CRC cells, which was linked to their improved cellular uptake and ability to target multiple cancer-related pathways. In contrast, GO NPs alone lacked cytotoxic effects. Gene expression analysis via qPCR revealed CeO$_2$:Ag/GO NPs significantly downregulated Zeb-1, VEGF, Cyclin-D1, and Twist compared to controls, altering cancer-related pathways more effectively than CeO$_2$:Ag NPs. Additionally, CeO$_2$:Ag/GO NPs significantly upregulated BAX and Caspase-1 while downregulating Bcl-2, implicating a more potent apoptotic response. This study highlights the advantage of CeO$_2$:Ag/GO NPs over CeO$_2$:Ag NPs in impeding CRC cell growth and inducing apoptosis, offering a promising foundation for innovative therapeutic strategies.

Introduction

Cancer, a prominent contributor to mortality, poses a substantial challenge to enhancing global life expectancy (Bray et al. 2021). Colorectal cancer (CRC) stands as the third most prevalent cancer and the second most widespread cause of death across multiple nations (Sung et al. 2021). Clear evidence demonstrates a global rise in early colorectal cancer incidence over the past 30 years (Burnett-Hartman et al. 2021). In the United States, CRC is regarded as the third highest cause of cancer-related mortality among both males and females (Siegel et al. 2020). Identifying individuals likely to have CRC through diagnosis and optimizing their screening procedures can significantly decrease both the morbidity and mortality associated with CRC. Conventional treatments include tumor resection, radiation therapy, and chemotherapy (Wang et al. 2021). While these approaches are effective, they often come with notable side effects. For instance, conventional chemotherapy primarily targets cancer cells by impeding mitosis and hindering DNA synthesis. Tissues in the gastrointestinal tract and hair follicles exhibit a rapid reproduction rate, which can occasionally lead to severe and fatal side effects (Hossen et al. 2019). Consequently, scientists are actively exploring novel methods to selectively eradicate cancer cells. Over the past 20 years, the utilization of nanoparticles (NPs) has become a crucial approach in cancer research and therapy. Nanomedicine, a rapidly advancing domain, employs NPs in various methodologies for diagnosing and treating cancer. Due to their distinctive physical traits such as electrical conductivity, stability, and optical properties, these particles are optimal for biotechnological applications. As a result, they find widespread use in medicine, pharmaceuticals, tissue engineering, and other fields (Khan et al. 2019).

NPs offer a more precise delivery mechanism for insoluble drugs to tumors, minimizing systemic side effects typically associated with conventional drug treatments (Sun et al. 2021). Moreover, certain NPs are employed in cancer therapy and tumor inhibition due to their cytotoxic and anticancer effects on cells (Raj et al. 2021). Metal NPs have garnered significant interest because of their versatility and multifunctional capabilities, setting them apart from other NP types. Barium, bismuth, calcium, cerium oxide, copper, gold, iron, magnesium, nickel, silver, titanium, and zinc metallic NPs have been recognized for their potential as anticancer treatments (Jeevanandam et al. 2022). Developing novel therapies for cancers, particularly CRC, is imperative. Prioritizing the creation of drugs with minimal side effects and heightened efficacy remains a crucial goal in this endeavor (Nowak-Sliwinska et al. 2019). The groundbreaking combination of cerium oxide (CeO_2) and silver NPs (Ag) with graphene oxide (GO) offers fresh insights into the design of NP-based therapies, potentially paving the way for innovative approaches in this field. The objective of this study was to investigate the impact of CeO_2:Ag/GO NPs on a colorectal cancer cell line. Initially, CeO_2:Ag NPs were produced using the hydrothermal synthesis technique, followed by the attachment of GO to enhance the cytotoxic effects of CeO_2:Ag NPs using the Hummers' technique. Subsequently, the toxicity of these NPs was evaluated. NPs influence cancer cells through various pathways, with apoptosis being a significant mechanism that plays a pivotal role in this process.

Tamtaji *et al. Cancer Nanotechnology* (2024) 15:62

Page 3 of 20

Numerous genes participate in apoptosis, among which caspase-3, Bax, and Bcl-2 are some of the most crucial. The impact of CeO_2:Ag/GO NPs on apoptosis was explored by targeting these genes using the qPCR technique.

Materials and methods

Materials

The chemicals utilized in the current study include cerium(IV) nitrate [$CeNO_3$, 99%], silver nitrate [$AgNO_3$, 99%], polyvinylpyrrolidone, ethanol, ammonia, hydrogen peroxide, potassium permanganate, graphite, hydrogen peroxide (30%), sulfuric acid (98%), ethanol, dimethyl sulfoxide (DMSO), and MTT (3-(4,5-dimethylthiazol-2-yl)−2,5-diphenyltetrazolium bromide), all sourced from Merck, were utilized without additional purification in this study.

Synthesis of CeO_2:Ag NPs

CeO_2:Ag NPs were produced using the hydrothermal synthesis technique. Initially, a solution of cerium(IV) with a concentration of 0.188 g was prepared. Subsequently, 0.1 g of the surfactant polyvinylpyrrolidone (PVP) was introduced to 10 ml of distilled water. Following that, 0.003 g of the obtained substance was dissolved in 5 ml of distilled water. The resulting mixture was then positioned on a magnetic stirrer and homogenized for 30 min at room temperature (25 °C). Afterward, the silver solution was gradually introduced drop by drop to the cerium solution while continuously mixing. After a 20-min incubation period, PVP was slowly added to the mixture while maintaining mixing for an additional 20 min. Subsequently, a mixture comprising 20 ml of water and ammonia in a 1:1 volume ratio was added drop by drop to the solution and mixed for 20 min. Following these steps, the solution underwent incubation for 24 h at 170 °C. The resulting product was divided into multiple tubes and centrifuged for 5 min at 4000 rpm. This procedure was repeated triplicate using deionized water and ethanol for washing purposes. Subsequently, the precipitate was placed on a watch glass and incubated for 5 h at 90 °C. Finally, the product was heated in laboratory furnaces for 4 h at 600 °C.

Synthesis of graphene oxide

Graphene oxide was produced using Hummers' technique with the following steps: initially, a combination of 1.0 g of graphite and 23 ml of sulfuric acid was stirred on a magnetic stirrer for 24 h at ambient temperature. Afterward, 0.1 g of sodium nitrate was introduced into the solution and stirred for 30 min. An ice bath was used to regulate the temperature, and after 30 min, the temperature was lowered to below 5 °C (specifically 2 °C). Subsequently, 3.0 g of potassium permanganate, hydrogen peroxide (30%), sulfuric acid (98%), and ethanol were gently incorporated into the mixture. Following the addition of potassium permanganate, the temperature was maintained between 35 and 45 °C for 30 min. Then, 46 ml of water was added to the mixture and stirred for 25 min. Afterward, the mixture received an additional 140 ml of water and 10 ml of hydrogen peroxide. Finally, the product underwent washing three times with water and ethanol at 4000 rpm for 5 min each time (Hummers and Offeman 1958; Hansora et al. 2015).

Characteristics of nanoparticles

The crystalline structures and formed phases of the NPs were identified using X-ray diffraction (XRD) analysis performed with an X-Pert-MPD X-ray diffraction device (Philips X'pert Pro MPP model). This analysis employed Cu-Kα1 (1.54060 Å) radiation, operating at a voltage of 40 kV and a current of 30 mA. The study involved diffraction over the 2θ range of 10°–80°, using a scanning increment of 0.05° and a stop time of 1 s. Fourier-transform infrared (FT-IR) spectroscopy was conducted with a Nicolet Magna−IR550 spectrophotometer, examining the functional groups present in KBr pellets over the 400–4000 cm^{-1} spectrum with a resolution of 1 cm^{-1}. Investigation of the dimensions and morphology of submicron powders was carried out using a scanning electron microscope (SEM) from TESCAN (TESCAN Mira 3–XMU model, Czech Republic) with energy-dispersive X-ray spectroscopy (EDX) capabilities. The chemical composition of the NPs was analyzed using EDX. A transmission electron microscope (TEM) with a Zeiss EM900 model was used to thoroughly examine the morphological structure of the NPs. Additionally, the dynamic light scattering (DLS) method, facilitated by Vasco/Cordouan Technologies, France, was used to measure the particle diameter and size distribution of the NPs.

In vitro anticancer activity of CeO$_2$:Ag/GO

Procurement and maintenance of cell lines

The colorectal cancer cell (C-26 cell line) and the HFF-2 (Human Foreskin Fibroblast 2) cell line as a normal cell were obtained from the Pasteur Institute (Iran). The cells were cultured in a growth medium containing 10% fetal bovine serum (FBS), penicillin (100 U/mL), and streptomycin (100 μg/mL) and maintained at 37 °C in a humidified environment with 5% CO$_2$.

Assessment of cytotoxicity

The cytotoxicity of GO, CeO$_2$:Ag, and CeO$_2$:Ag/GO NPs was assessed using the MTT assay in C-26 colorectal carcinoma cells. Initially, 5×10^3 cells were seeded per well in a microtiter plate and incubated for 24 h. The cells were then treated with varying doses (0–100 μg/mL) of different NPs, followed by an additional 24-h incubation in a CO$_2$ incubator. After washing, the cells were cultured in a complete culture medium for an additional 24 h at 37 °C. After this incubation period, 20 μL of MTT solution was added to the cells, and the mixture was incubated at 37 °C for 4 h. Following this, 100 μL of DMSO was added, and after dissolving the crystals formed with DMSO, the absorbance was measured at 570 nm using a spectrophotometer.

Gene expression

Quantitative polymerase chain reaction (qPCR) was employed to assess the transcriptional expression of the Bax, Bcl-2, Caspase-1, ZEB-1, VEGF, Cyclin-D1, and Twist genes, with GAPDH used as the reference gene. This allowed for the evaluation of mRNA levels in treated cells across various experimental groups. Total RNA extraction was performed using the Yekta Tajhiz kit, and the concentration was determined using a NanoDrop device. In each sample, 200 ng of total RNA was converted into

cDNA using Oligo-dT and random primers, with the Parstous cDNA kit. The subsequent step involved real-time PCR utilizing the generated cDNAs, and specific primers for Bax, Bcl-2, Caspase-1, ZEB-1, VEGF, Cyclin-D1, Twist, and SYBR Green dye. The device's heating schedule consisted of three stages. The initial stage involved a 5-min duration at 95 °C to denature the cDNA molecules. The second stage consisted of 45 cycles at 95 °C for 15 s for denaturation, followed by 10 s at 60 °C for annealing, and 9 s at 72 °C for extension. The reactions were conducted in triplicate, and all analyses were performed using relative quantification methods, normalized to GAPDH as the housekeeping gene.

Results

Nanoparticle characteristics

XRD patterns

The XRD spectra of the NPs, as shown in Fig. 1, correspond to CeO_2, CeO_2OH, GO, and CeO_2:GO, confirming the successful formation of all samples and displaying pronounced crystallinity. To eliminate redundant peaks observed in Fig. 1b, CeO_2 was calcined for 4 h at 600 °C. The XRD pattern of calcined CeO_2 NPs spans the 2θ range of 10–80° (Fig. 1a). All identifiable peaks correspond to a fully cubic configuration of CeO_2 (space group: $Fm\bar{3}m$) with a lattice constant of a = 5.411 Å, in agreement with the JCPDS (Joint Committee on Powder Diffraction Standards) file for CeO_2 (JCPDS 00–034–394) (Wang et al. 2018). As clearly evident in the XRD pattern of CeO_2, the most intense diffraction peak occurs at 2θ = 28.660°, originating from the (111) lattice plane within the face-centered cubic structure of CeO2. The GO XRD spectra display three prominent
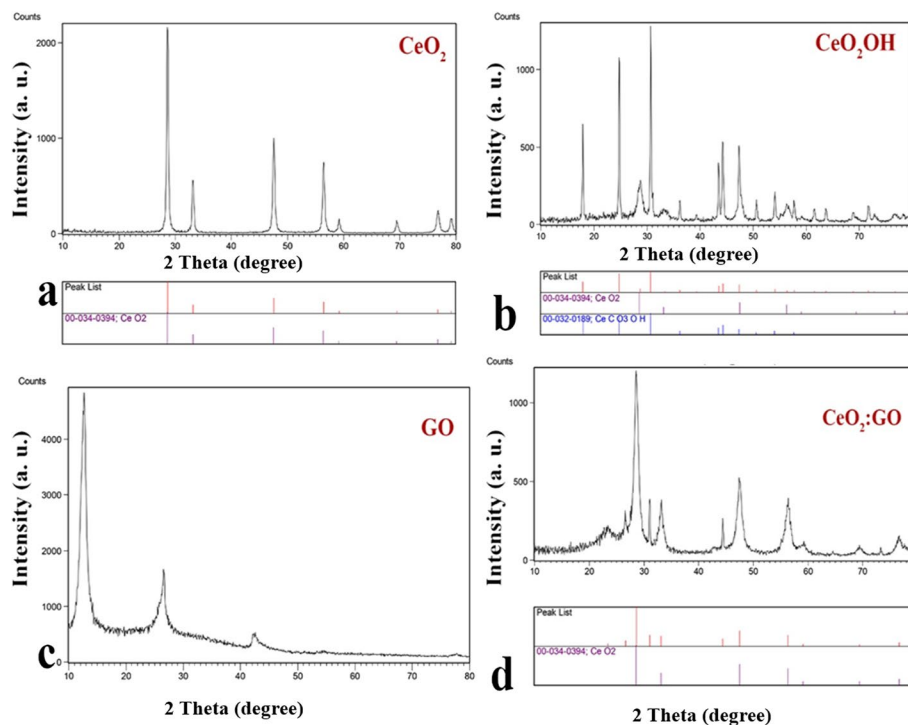
**Fig. 1** The XRD patterns of different nanoparticles: **a** CeO_2, **b** CeO_2OH, **c** GO, and **d** CeO_2:GO

peaks at $2\theta = 12$, 26, and 43, primarily indexed as 001, confirming the layered structure of GO (Fig. 1c). Upon combining CeO_2 with GO (Fig. 1d), the XRD pattern and crystalline structure remained unchanged. However, a slight shift in peak positions was observed compared to Fig. 1a. The XRD pattern of CeO_2:GO NPs shows a combination of peaks from both CeO_2 and GO. The presence of sharp peaks indicates the retention of the cubic structure of CeO_2, while the broad peak around $2\theta = 12°$ corresponds to GO, confirming the successful formation of the CeO_2:GO nanocomposite. The slight shift in the CeO_2 peaks suggests an interaction between CeO_2 and GO, potentially due to the attachment of CeO_2 NPs to the GO sheets. This combination of peaks indicates that the CeO_2:GO NPs retain the crystallinity of CeO_2 while integrating the layered structure of GO.
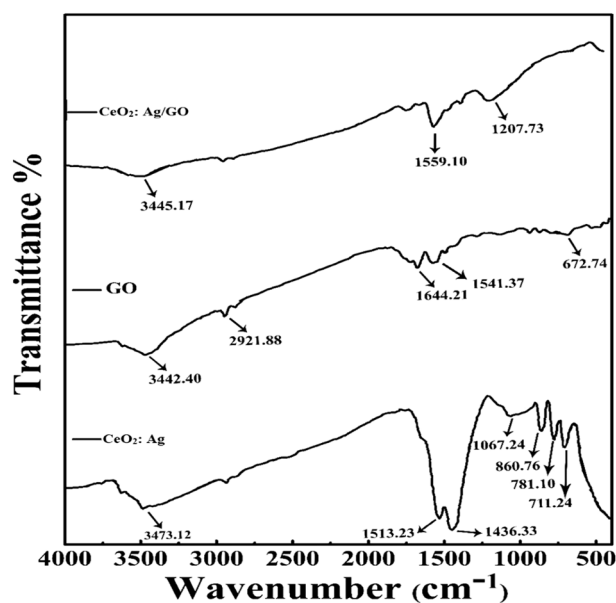
EDX analysis

EDX analysis complements the XRD pattern by providing precise details regarding NPs quantity and elemental composition, indicated in both weight and atomic percentages. In Fig. 2, it is evident that the synthesized NPs exhibit high purity with minimal impurities. Additionally, the figure elucidates the percentage composition of each element present in the samples. In Fig. 2a, it is shown that 66.38% of GO is composed of carbon, while 32.62% consists of oxygen. Meanwhile, Fig. 2b demonstrates that CeO_2:Ag NPs contain 44.17% oxygen, 54.96% cerium, and 0.87% silver. Finally, the carbon, oxygen, cerium, and silver contents of CeO2:Ag/GO NPs were 73.49%, 16.13%, 1.01%, and 0.37%, respectively.

FT-IR spectral analysis

Figure 3 displays the FT-IR spectra for analyzing the adsorption species on the surfaces of the as-synthesized CeO_2, CeO_2:Ag, and CeO_2:Ag/GO NPs. The spectral profile of CeO_2:Ag NPs exhibits a subtle band around 3473 cm^{-1}, attributed to the O–H stretching vibration mode of adsorbed water from moisture. The intricate bands observed at approximately 1513 cm^{-1}, 1436 cm^{-1}, and 1067 cm^{-1} arise from undesirable residues in the sample, associated with CH_2 bending, C–H bending vibration, and C–O stretching vibration, respectively. The absorption bands at 711 cm^{-1} and 781 cm^{-1} indicate metal–oxygen bonds (Lin et al. 2006). Additionally, the faint absorption band observed at 860 cm^{-1} is attributed to the stretching vibration of Ce–O (Zhang et al. 2005; Sharma et al. 2020; Kumar et al. 2010). In the GO spectrum, the broad peak at 3445.39 cm^{-1} is ascribed to OH stretching vibrations, while the peak at 1644 cm^{-1} is assigned to the bending vibration of absorbed water molecules and contributions from the sp^2 characteristics (Dezfuli et al. 2015). The peak
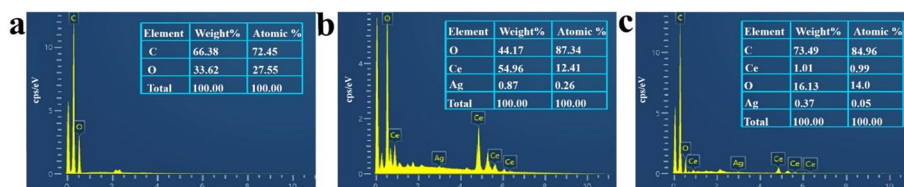
**Fig. 2** EDX analysis of synthesized **a** GO, **b** CeO_2:Ag and **c** CeO_2:Ag/GO nanoparticles

Fig. 3 FT-IR analysis of GO, CeO$_2$:Ag, and CeO$_2$:Ag/GO nanoparticles

at 2921 cm^{-1} indicates sp^3 C–H bonding, signifying that the product was generated in an acidic phase, confirming the presence of carboxylic acid in its structure (Spitalsky et al. 2011). The significant band at 3445 cm^{-1} is linked to the vibration of the OH group, corresponding to residual water and/or hydroxyl groups. The peaks observed at 1573 cm^{-1} correspond to the C＝C stretching mode of the quinoid rings and C＝OH, indicating the presence of partial functional groups in GO (Duan et al. 2016). The presence of peaks at 1207 cm^{-1} is attributed to the stretching vibration modes of C–O–C, confirming the coexistence of both CeO$_2$ and GO-Ag NPs in the CeO$_2$:Ag/GO nanocomposite (Sun et al. 2023).

X-ray mapping analysis

The X-ray mapping analysis illustrates the distribution of individual elements within the GO, CeO$_2$:Ag, and CeO$_2$:Ag/GO NPs. Figure 4a shows the uniform distribution of carbon and oxygen within the GO sample, indicating a homogenous elemental spread in the graphene oxide. However, Fig. 4b displays a much weaker X-ray mapping signal in the center of the CeO$_2$:Ag sample compared to the background. This unusual observation may be due to the aggregation of silver NPs in localized regions, leading to inconsistent distribution and, consequently, signal intensity variations. Aggregation of silver could result in diminished signal density in specific areas where the concentration of Ag particles is higher, creating apparent discrepancies in the mapping signal. In contrast, Fig. 4c confirms the successful synthesis of the CeO$_2$:Ag/GO NPs, demonstrating a more uniform and even distribution of all constituent elements within the structure, attributed to the interaction between CeO$_2$ and GO, which helps to reduce the aggregation effect seen in CeO$_2$:Ag.
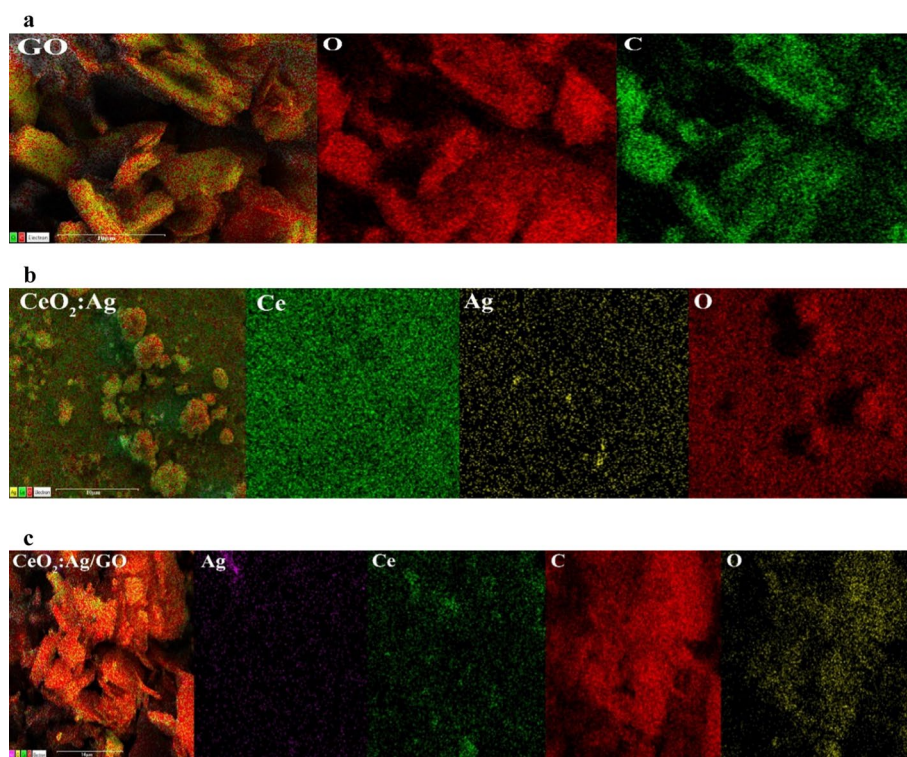
Fig. 4 X-ray mapping analysis of fabricated nanoparticles: **a** GO, **b** CeO$_2$:Ag, and **c** CeO$_2$:Ag/GO

Microstructure characteristics of nanoparticles

The microstructural properties of CeO$_2$:Ag, pure GO, and CeO2:Ag/GO NPs were studied using the SEM technique. In Fig. 5a, b, CeO$_2$:Ag/GO NPs are visible, where silver NPs are decorated onto CeO$_2$ particles and are attached to the graphene oxide sheets. The size of the CeO2:Ag NPs has notably decreased after the composite formation with GO compared to the observations of CeO$_2$:Ag NPs alone, as depicted in Fig. 5c. In this image, the agglomeration of CeO$_2$:Ag NPs is evident, with particle sizes distinctly within the nanoscale range. Figure 5c shows the structure of CeO$_2$:Ag NPs, where silver atoms are doped into the CeO$_2$ lattice. These NPs exhibit a spherical shape, and the majority measure less than 200 nm in size. The agglomerated particles in this figure highlight the structural and morphological characteristics of the CeO$_2$:Ag NPs without any graphene oxide present. Regarding the reduced size of CeO$_2$:Ag NPs, while SEM images were taken at different magnifications, the scale bars in the images indicate a reduction in size following their combination with graphene oxide, as shown in Fig. 5a, b. Additionally, Fig. 5d presents CeO$_2$:Ag/GO NPs, where the CeO$_2$:Ag NPs are uniformly dispersed over graphene oxide sheets. The presence of graphene in the composite aids in the reduction of agglomeration and results in a more homogeneous distribution of CeO$_2$:Ag particles on the graphene surface. Figure 5e displays pure GO sheets without the presence of any NPs, providing a contrast to the nanocomposites shown in Fig. 5a, b.
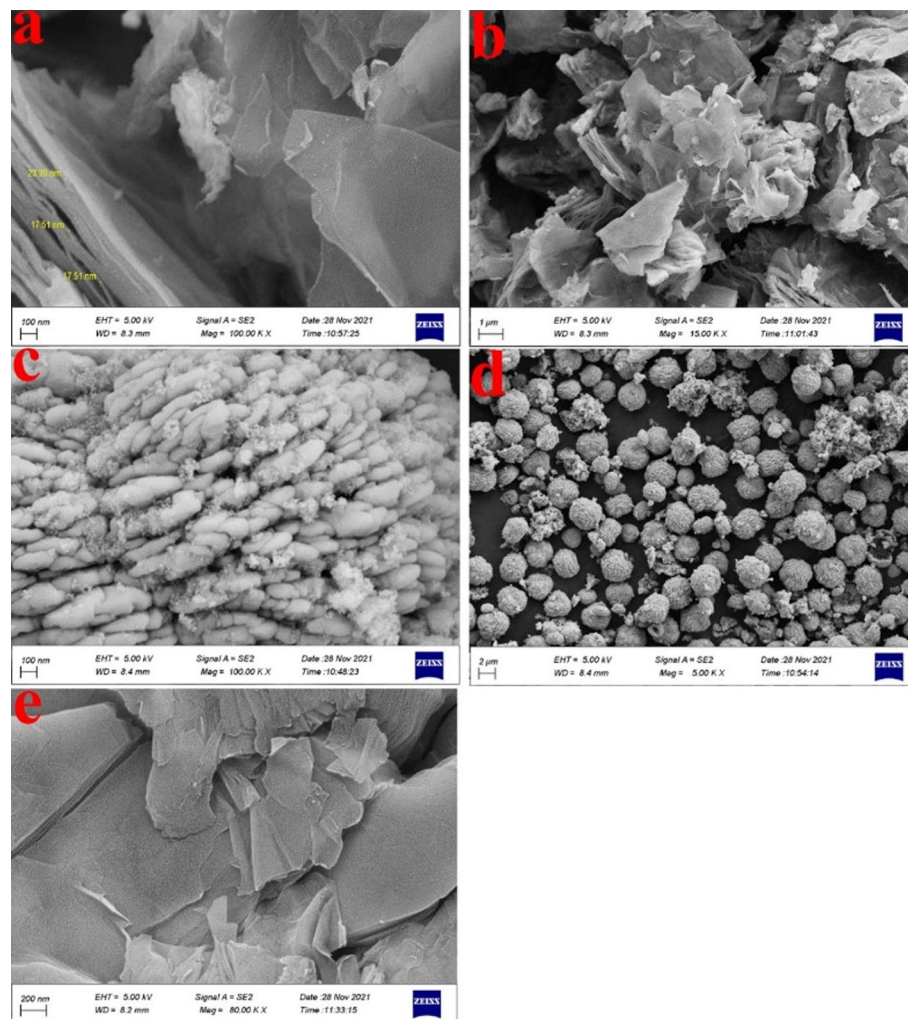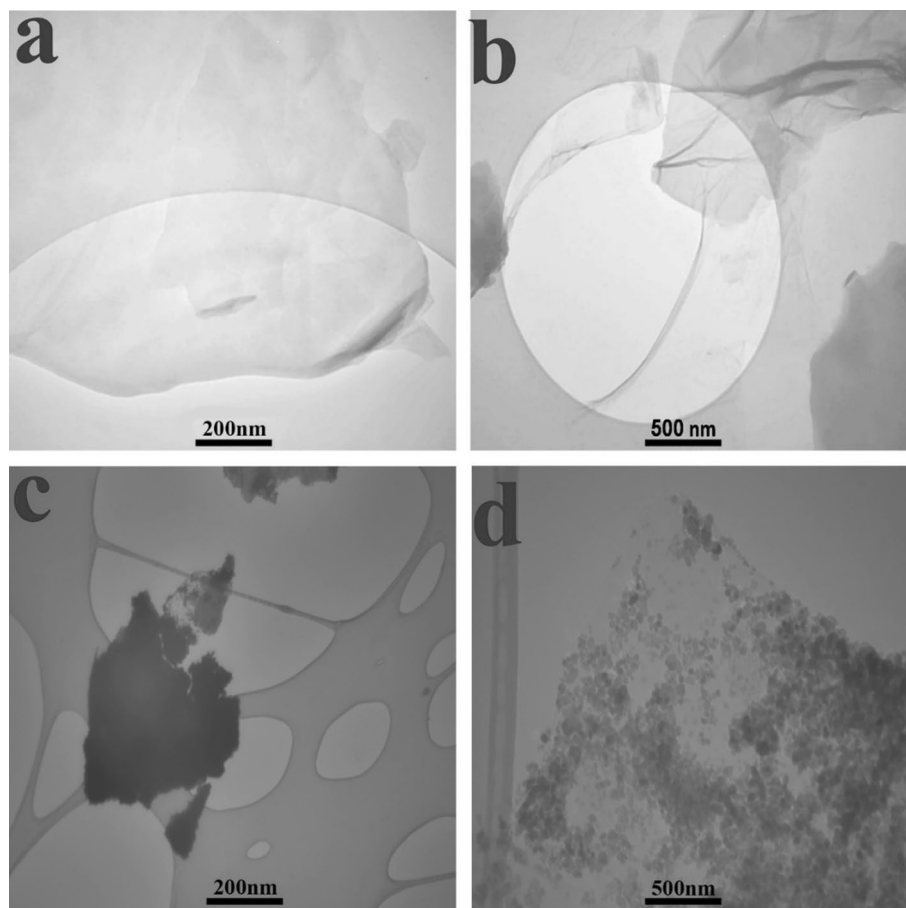
Fig. 5 SEM analysis of nanoparticles: **a**, **b**, and **d** CeO_2:Ag/GO, **c** CeO_2:Ag, and **e** graphene oxide

TEM imaging

The dimensions and morphology of the synthesized NPs were examined through TEM analysis. TEM micrographs of CeO_2:Ag/GO NPs are shown in Fig. 6c, d. From these micrographs, the measured particle size of CeO_2:Ag NPs appears to be approximately 150–200 nm. The images clearly depict the placement of CeO_2:Ag NPs onto GO sheets, with an apparent accumulation of CeO_2:Ag NPs, as shown in Fig. 6c, d. Meanwhile, graphene sheets are visible in both Fig. 6a, b.

Particle size

Dynamic light scattering (DLS) is a method used to determine the hydrodynamic diameter of NPs in a solution. It provides insights into the state of NPs aggregation within the solution. The DLS analysis conducted on CeO_2:Ag/GO NPs revealed an average particle diameter of approximately 20 nm (Fig. 7).

Fig. 6 TEM micrograph of nanoparticles: **a** and **b** graphene oxide, **c** and **d** CeO$_2$:Ag/GO
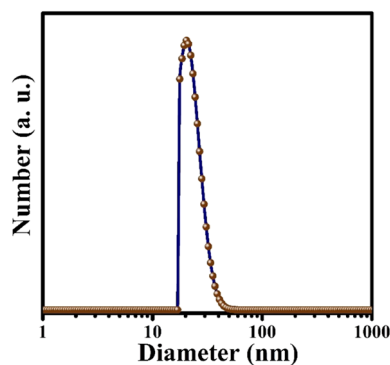
Fig. 7 DLS analysis of CeO$_2$:Ag/GO nanoparticles

Evaluating cytotoxic effects of fabricated nanoparticles through MTT assay

The MTT method is a colorimetric assay designed to measure the reduction of MTT by the succinate dehydrogenase enzyme present in the mitochondria of living cells. This assay is widely used to assess cytotoxicity and determine the viability of cells treated with various compounds by measuring the metabolic activity of viable cells. The MTT reagent

permeates the cell and enters the mitochondria, where it is reduced to form an insoluble, purple-colored formazan. This conversion occurs due to mitochondrial enzyme activity in viable cells. The purple formazan is then dissolved in DMSO, and its absorbance is measured at a wavelength of 570 nm using a spectrophotometer. The reduction of MTT and similar tetrazolium dyes correlates with cell metabolism: reduced metabolic activity leads to lower MTT reduction, while higher activity results in increased reduction.

This investigation involved applying varied doses of CeO_2:Ag/GO, CeO_2:Ag, and pure GO NPs to CRC cells (Fig. 8). After 24 h, cell viability percentages were assessed using the MTT assay. The findings indicated that both CeO_2:Ag and CeO_2:Ag/GO NPs significantly inhibited the growth and proliferation of C26 cells, with IC50 values of 13.76 and 6.8 μg/mL, respectively (Fig. 8a, b). The more pronounced inhibitory effect of CeO_2:Ag/GO can be attributed to the role of GO in enhancing the interaction of the NPs with cancer cells. GO acts as a carrier platform that improves the dispersity and stability of CeO2 and Ag NPs, which in turn facilitates a more efficient delivery of the active components to the cancer cells. While CeO_2:Ag NPs alone displayed significant cytotoxic effects, the integration of GO into the CeO_2:Ag/GO nanocomposite likely enhances the overall efficacy of the NPs. GO's layered structure allows for better attachment and distribution of CeO_2 and Ag NPs on the cell surface, leading to improved cellular uptake
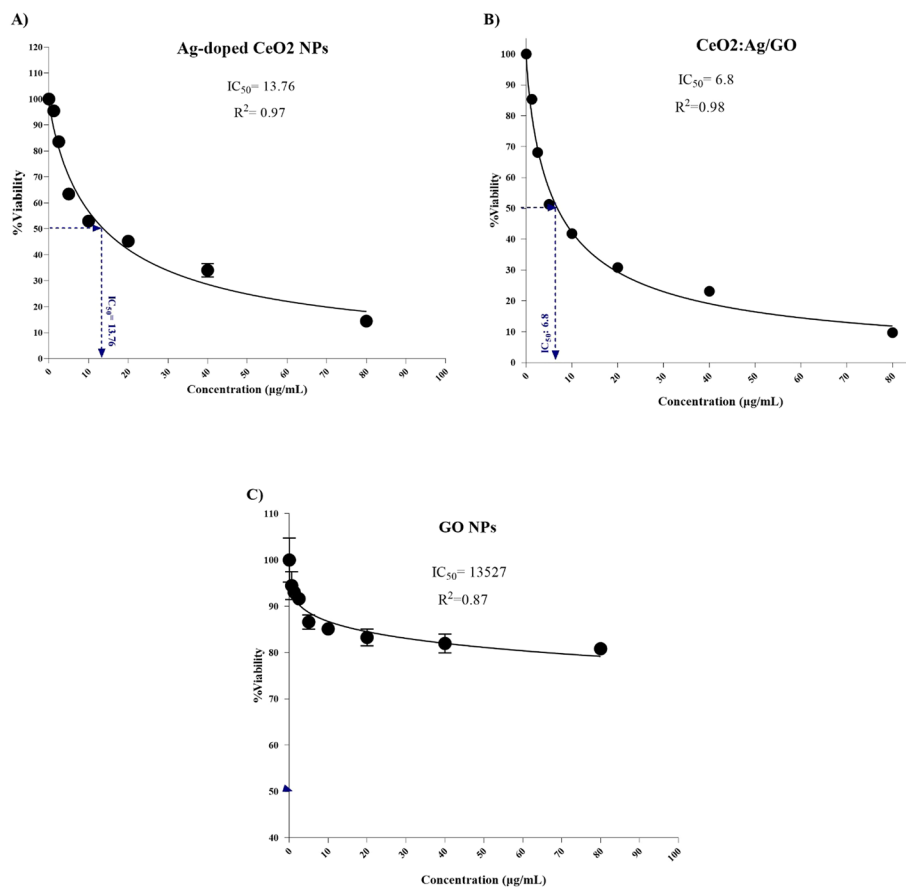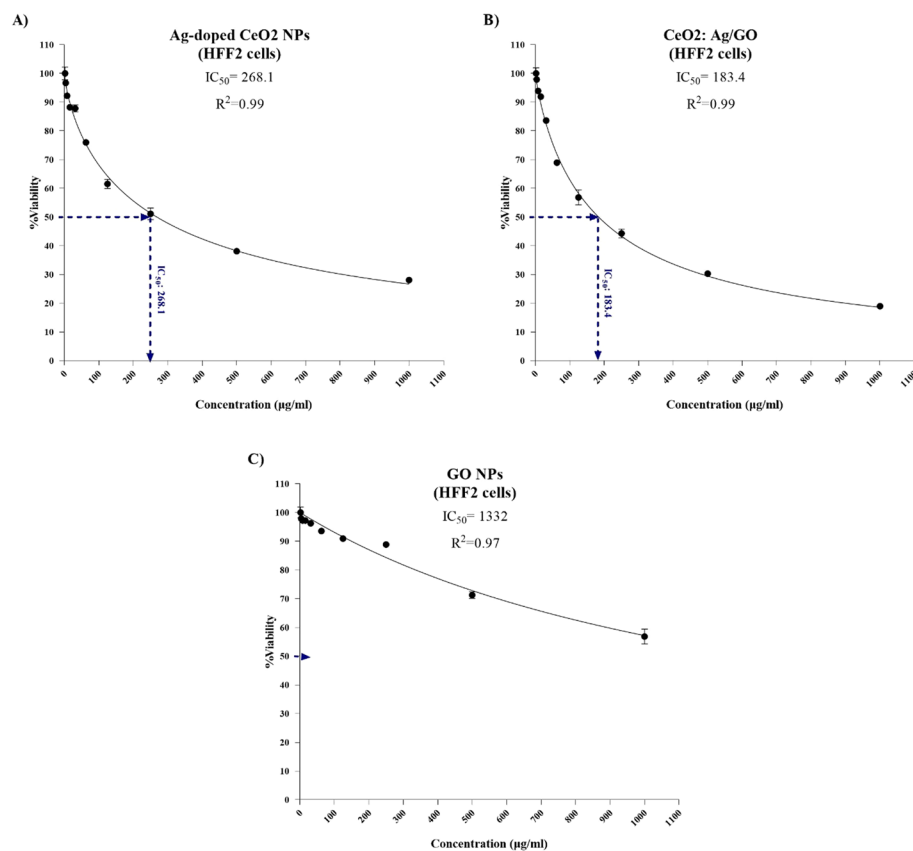

Fig. 8 Cell viability assay of **a** CeO_2:Ag/GO, **b** CeO_2:Ag, and **c** graphene oxide against C-26 cells

and interaction. This synergistic effect results in a lower IC50 value for CeO_2:Ag/GO, indicating greater cytotoxicity compared to CeO_2:Ag NPs alone. Conversely, GO NPs alone did not exhibit cytotoxic effects on the cells (Fig. 8c), underscoring the importance of its role as a facilitator for the combined therapeutic action of CeO_2 and Ag in the CeO_2:Ag/GO composite rather than as a standalone therapeutic agent. We addressed the sensitivity of normal cells in the context of our study. We observed no cytotoxic effects on HFF-2 cells in the treatment groups (Fig. 9). We emphasized that this does not necessarily imply a complete lack of sensitivity in all normal cells. We clarified that differential toxicity can occur and discuss the implications of our findings regarding normal cell responses.

Gene expression

A multi-analyte real-time PCR was conducted to discern the activated pathways triggered by NPs in cells pre-treated with CeO_2:Ag/GO, CeO_2:Ag, and pure GO NPs. The aim was to evaluate gene expression levels in crucial pathways linked to human cancer cell survival in C-26 colorectal cancer cells exposed to these NPs. The expression levels of Bax, Bcl-2, Caspase-1, Cyclin-D1, Twist, VEGF, and ZEB-1 in human colorectal cancer cells were investigated using RT-PCR (Figs. 10, 11). The analysis indicated a notable reduction in the mRNA expression of the VEGF gene in the CeO_2:Ag/GO group

Fig. 9 Cell viability assay of **a** CeO_2:Ag/GO, **b** CeO_2:Ag, and **c** graphene oxide against HFF-2 cell line
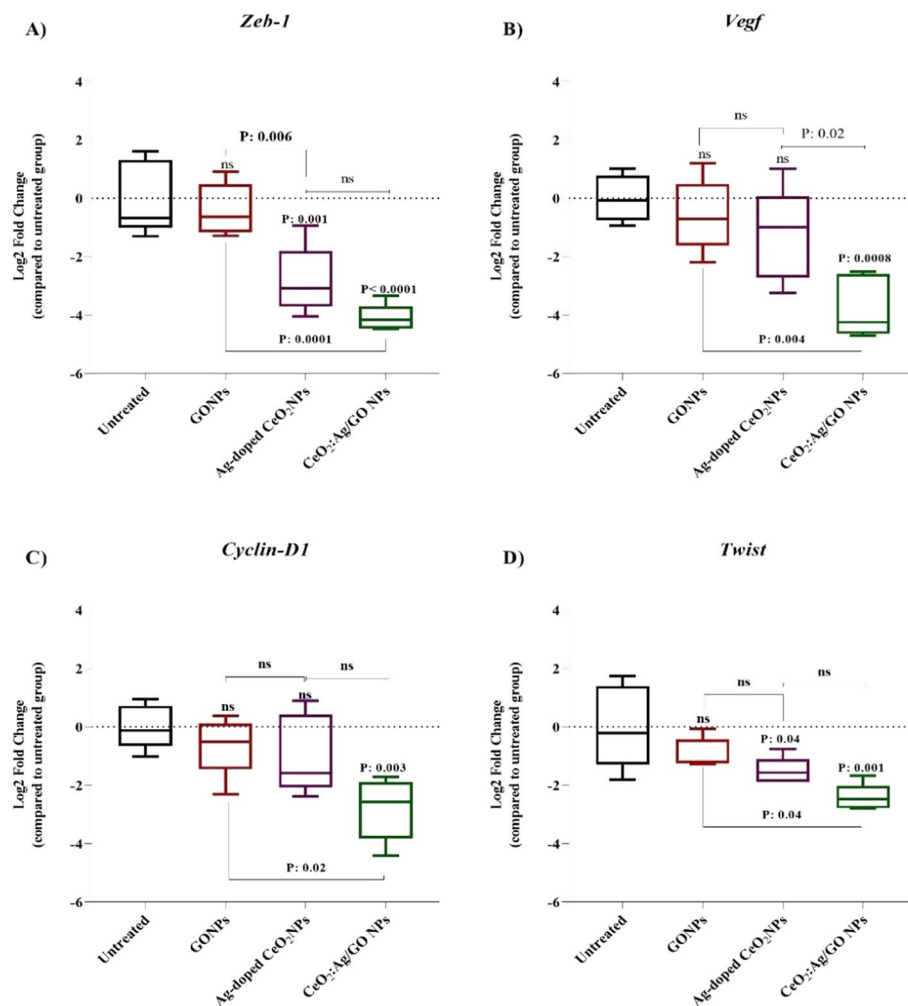
Fig. 10 Using graphene oxide (GO), CeO_2:Ag, and CeO_2:Ag/GO nanoparticles, gene expression and functional assays were conducted against C-26 cells, evaluating the fold difference in mRNA expression of **a** Zeb, **b** VEGF, **c** Cyclin-D1, and **d** twist across colorectal cancer cell lines via quantitative real-time polymerase chain reaction (qRT-PCR). The data are presented as mean values with standard deviation (mean ± SD), and "ns" denotes insignificance in the observed results

($p = 0.02$ compared to the CeO_2:Ag group), emphasizing the impact of the combined therapy involving GO and CeO_2:Ag. The treatment with CeO_2:Ag/GO notably diminished the gene expression of ZEB-1, VEGF, Cyclin-D1, and Twist ($p < 0.0001$, $p = 0.0008$, $p = 0.003$, and $p = 0.001$, respectively) compared to the control group. Ag-doped CeO_2 reduced the levels of ZEB-1 ($p = 0.001$) and Twist ($p = 0.04$), but did not significantly impact VEGF and Cyclin-D1 expression. Interestingly, GO NPs alone did not significantly affect gene expression in any of the groups.

Discussion

CeO2 NPs have demonstrated potential in modulating oxidative stress in various conditions such as retinal degeneration, neurological disorders, ischemia, heart disease, diabetes, gastrointestinal inflammation, liver disease, and cancer. This versatile behavior
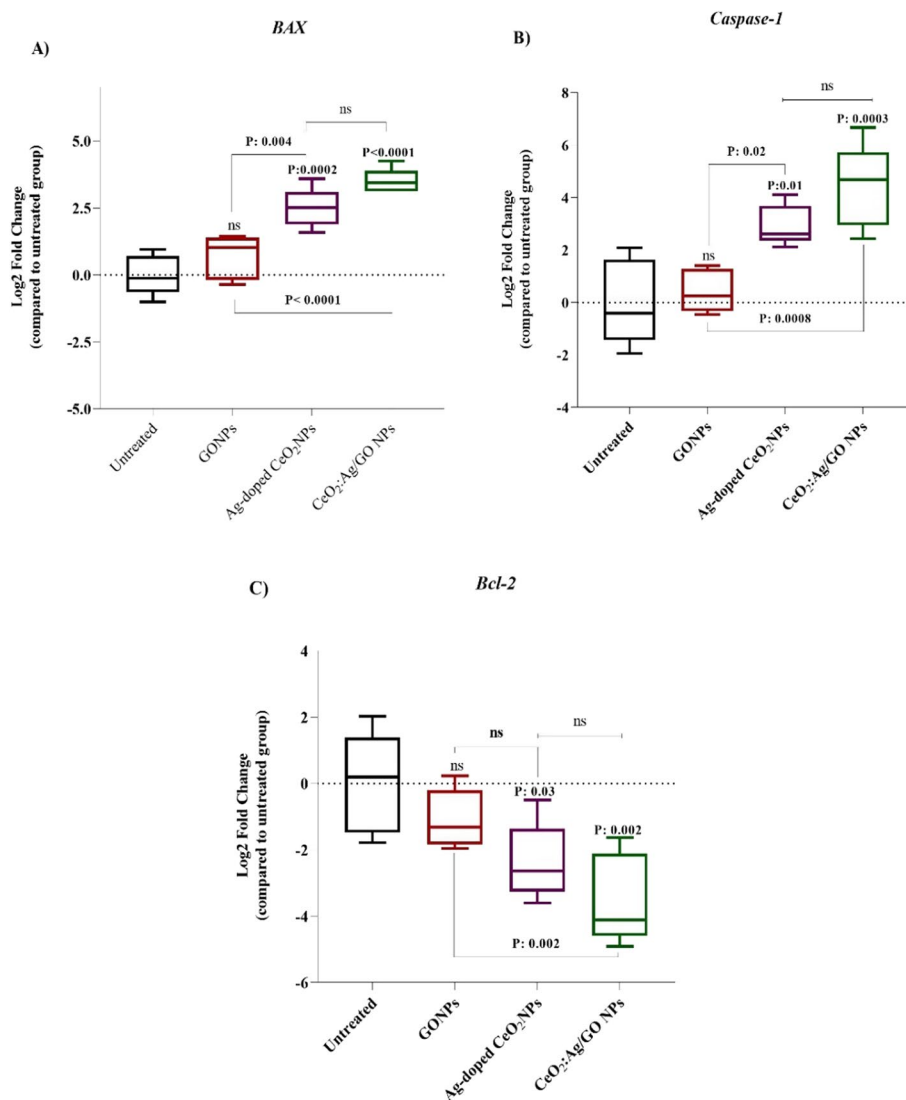
Fig. 11 Assessing graphene oxide (GO), CeO2:Ag, and CeO2:Ag/GO nanoparticles, gene expression and functional tests were performed on C-26 cells, analyzing the mRNA expression fold changes of **a** Bax, **b** Caspase-3, and **c** Bcl-2 across colorectal cancer cell lines using qRT-PCR. Results are expressed as mean values ± standard deviation (mean ± SD), with 'ns' indicating statistical insignificance in the findings

suggests that CeO_2 could serve as a promising candidate for the targeted production of anti-tumor drugs (Inbaraj and Chen 2020). Research has shown that cerium oxide induces considerable oxidative stress in human bronchial and hepatocellular carcinomas (Marzi et al. 2013; Lin et al. 2006). In adenocarcinoma cells (A549), CeO2 has been observed to increase the generation of reactive oxygen species (ROS), consequently reducing the cell's antioxidant levels and leading to apoptotic cell death (Mittal and Pandey 2018). There is evidence that CeO2 NPs can induce apoptosis by activating caspases and causing chromosomal DNA fragmentation. Additionally, they elevate ROS levels in colorectal cancer cells without causing harm to normal cells (Datta et al. 2020). Silver NPs (Ag NPs) also stand out as highly effective NPs, renowned for their antibacterial and anticancer properties (Kovács et al. 2022). The primary distinction between silver

NPs and small-molecule drugs lies in their structure, which helps mitigate the severity of undesirable side effects (Maeda et al. 2013).

Research has established that the optimization effects of Ag NPs rely on several factors, including shape, size, capping material (Danhier et al. 2010), and the utilization of folic acid-targeted Ag NPs (Kovács et al. 2022). The activation of various intercellular molecular pathways has been suggested for Ag NPs, encompassing Ag NP-induced anti-proliferative signaling, classical apoptotic pathways, DNA damage response, MAP kinase stimulation, oxidative stress, sustained autophagy induction, and ER stress (Simard et al. 2016; Chen et al. 2020). In research conducted by Valenzuela-Salas, Girón-Vázquez (Valenzuela-Salas et al. 2019), the AgNP-TAT combination was applied in both in vivo and in vitro methods within a melanoma cancer model. The observed effects demonstrated reduced tumor growth and size. They also employed silver NPs in melanoma cancer, leading to apoptosis and subsequent reduction in tumor growth. Furthermore, the silver NPs prompted an overproduction of ROS, eventually leading to cancer cell death (Valenzuela-Salas et al. 2019). In a separate study by Zhang, Choi (Zhang et al. 2015), the inhibitory impact of silver NPs was observed, resulting in a decrease in the proliferation and self-renewal of spermatogonial stem cells (SSCs) (Zhang et al. 2015). In another study by Li, Sun (2012), uniform silver NPs were examined for a quantitative investigation of cytotoxicity. The impact of silver NPs on cell viability, apoptosis, necrosis, and ROS production in human lung fibroblasts was thoroughly explored using silver NPs of varying sizes and doses. The research revealed a notable escalation in cytotoxicity correlating with a reduction in the size of silver NPs and an increase in their dosage. These outcomes were linked to the creation of monodispersed silver NPs of varying sizes (Li et al. 2012).

In a study by Hadrup, Loeschner (2012), it was concluded that both silver ions and silver NPs influence neurotransmitters in the brains of rats. Silver ions and silver NPs also trigger apoptosis in vitro through the death receptor and mitochondrial pathways, exerting a neurotoxic effect. In a study conducted by Jeyaraj, Sathishkumar (2013), the effects of Ag NPs on breast cancer were investigated. The findings indicated that silver NPs induce DNA damage by generating ROS, suggesting that the synthesized silver NPs might serve as a potential alternative chemotherapy agent (Jeyaraj et al. 2013). In separate research by Govender, Phulukdaree (2013), the effects of AgNPs were observed, including heightened activity of caspases 3/7/9, escalated mitochondrial depolarization, and elevated levels of Bax and Smac/Biablo in lung carcinoma cells. The study by Mata, Nakkala and Sadras (2015) explored the impact of silver NPs on colon cancer. The findings revealed that AIAg NPs triggered apoptotic cell death at a remarkably low concentration in colon cancer cells by elevating intracellular ROS production and reducing mitochondrial membrane potential, resulting in DNA fragmentation and cell cycle arrest (Mata et al. 2015). Additionally, there are promising results regarding the anticancer and antioxidant effects of GO composites. For instance, Ag NPs decorated with graphene oxide NPs diminished colon cancer cell growth through a radiosensitizing mechanism (Habiba et al. 2019).

Graphene oxide (GO) is a chemical similar to graphene, but it incorporates oxygen-based functional groups into its structure. GO has garnered significant attention due to its distinctive electrical, mechanical, and thermal characteristics (Liao et al. 2011). There

is controversy regarding the anticancer effects of GO. Findings from one study suggest that GO does not exhibit cytotoxic effects on its own (Inbaraj and Chen 2020). However, when combined with certain drugs, such as doxorubicin, it significantly enhances the drug's cytotoxicity compared to the effects of pure doxorubicin (Sun et al. 2023). On the other hand, multiple research studies have demonstrated GO's ability to trigger oxidative stress and elevate ROS levels (Duan et al. 2016). Moreover, GO is recognized for its involvement in activating diverse intracellular pathways, such as AMPK/mTOR/ULK-1, which are associated with autophagy and apoptosis (Shen et al. 2022). While debates persist regarding graphene oxide's anticancer effects, its efficacy as a co-drug to enhance cytotoxicity remains unquestionable. In a particular study, both Ag NPs and Ag-GO NPs elevated the ratio of Bax to Bcl-2 and increased intracellular ROS. However, Ag NPs demonstrated the highest efficacy in increasing the Bax/Bcl-2 ratio, whereas Ag-GO further enhanced ROS formation (Ganjouzadeh et al. 2022). Recent findings suggest that CeO_2 NPs impact oxidative stress in conditions such as retinal degeneration, neurological disorders, ischemia, heart disease, diabetes, gastrointestinal inflammation, liver disease, and cancer. Thus, CeO_2 emerges as a viable candidate for the development of targeted anti-tumor medications (Casals et al. 2020). In 2020, research conducted by Pandiyan Nithya et al. employed silver and gold NPs doped with CeO_2 in the context of cervical cancer. The findings revealed a notable impact of these NPs, indicating a dose-dependent effect. Silver and gold NPs doped with CeO_2 triggered ROS generation and impeded tumor cell growth. Therefore, Ag–Au/CeO2 NPs possess both antibacterial and anticancer attributes (Nithya and Sundrarajan 2020). In research conducted by Melissa S. Wason and her team, CeO_2 NPs were found to induce JNK activation, facilitating apoptosis in pancreatic cancer cells (Wason et al. 2018). In a study by Singh, Gupta (2018), combining GO with doxorubicin revealed enhanced effectiveness compared to using pure doxorubicin alone. According to the study by Jafarinejad-Farsangi, Hashemi (2021), GO exhibits no toxic effect on its own, but in combination with a drug, it can augment the drug's toxicity. However, controversy surrounds the antibacterial and anticancer properties attributed to GO. Graphene-based materials like GO have garnered significant attention in biosensor applications due to their robust signal output and immense potential for rapid industrial growth. The exceptional conductivity and mechanical resilience of graphene, coupled with its heightened reactivity to chemical molecules, make it particularly appealing. The existence of surface waves, whether inherent or induced, presents another variable that, if effectively utilized, holds immense potential (Yildiz et al. 2021).

The Wnt/β-catenin signaling axis plays a crucial role in the development of CRC (Ji et al. 2022). Cyclin D1 and β-catenin are primary components involved in both the cell cycle and carcinogenesis. The Wnt/β-catenin signaling pathway regulates the transcriptional programs essential for the growth and development of various tissues. Multicellularity is vital for proper biological function, and dysregulated activity within the Wnt/β-catenin complex can lead to cancer, particularly colorectal cancer (Jung et al. 2015). Wnt signaling is essential for governing stem cell growth and maintaining tissue homeostasis (Clevers et al. 2014). Additionally, this pathway is fundamental in cell proliferation, cell fate determination, cell migration, and establishing cell polarity during embryonic development. Wnt ligands bind to Frizzled receptors and 5/6

protein receptors, which are linked to low-density lipoprotein receptors. By inhibiting the degradation complex involving adenomatous polyposis coli (APC), axin, casein kinase 1, and glycogen synthase kinase, Wnt signaling stabilizes the β-catenin protein, consequently initiating the activation of β-catenin-targeted gene transcription (Clevers and Nusse 2012). Common mutations in the genetic components of the Wnt signaling pathway are strongly linked to human colon cancer and CRC. Research in mouse models indicates that genetic mutations causing heightened Wnt signaling activity result in mammary tumors and intestinal adenomas. This disruption in Wnt signaling significantly influences the onset of intestinal tumors. Mutations in key components of Wnt signaling contribute to the hyperactivation of the Wnt/β-catenin signaling pathway. For instance, over 70% of colorectal cancer cells exhibit significant mutations in elements of the Wnt signaling pathway, such as APC, AXIN1, or β-catenin/CTNNB1 (Kasprzak 2020). It has also been demonstrated that hyperactivation of Wnt signaling in CRC cells is triggered by silencing Wnt signaling antagonists at the transcriptional level. Of the 19 Wnt ligands in mammals, Wnt1, Wnt3A, Wnt8, and Wnt10 activate the canonical Wnt signaling pathway through β-catenin, which is recognized as a canonical Wnt ligand. Studies have revealed that heightened expression of Wnt3A is linked to the development of intestinal tumors (Kasprzak 2020). Thus, β-catenin serves as the central mediator of this pathway, undergoing proteasomal degradation in the absence of Wnt (Roche et al. 2008). In various malignancies, β-catenin has been identified as an oncogene with a significant role. One of the molecules regulated by β-catenin, Cyclin D1, stands out as a potential stimulator of the carcinogenic pathway.

Clinical samples of colon cancers have been examined to explore the correlation between β-catenin and Cyclin D1 (Utsunomiya et al. 2001). Cyclin D1 is a key regulator in the cell cycle, particularly in the G1 phase, serving as an oncogene known for promoting malignant transformations. In human cancers, elevated levels of Cyclin D1 have been frequently observed in clinical studies, correlating with the tumor's malignant potential (Utsunomiya et al. 2001). Furthermore, the impact of epithelial–mesenchymal transition (EMT) programs on cell proliferation and survival has been associated with the development of tumors. During EMT, epithelial cells gradually transform in morphology and adopt biochemical traits characteristic of a more mesenchymal state. Transcription factors play a crucial role in promoting cell plasticity, aiding tumor advancement. EMT transcription factors (EMT-TFs) have been linked to unfavorable clinical outcomes in various cancers, regardless of their origin in epithelial or non-epithelial tissues. EMT does not follow a singular pathway; it involves EMT-TF families such as SNAIL, SLUG, TWIST, and ZEB, which are tissue-specific and contribute to its diverse biological nature. Various tumor events associated with EMT can converge toward similar phenotypic outcomes in clinical samples (Umar 2014). TWIST and ZEB1, both members of the ZEB family derived from EMT-TFs, serve as consistent markers in the progression of tissue malignancies, including colon cancer (Wu et al. 2019). Cyclin D1, encoded by the CCND1 gene, is a cell cycle regulatory protein associated with multiple cancers, including colon cancer. Increased expression of this gene has been shown to be related to metastasis and proliferation of CRC cells (Albasri et al. 2019).

Tamtaji *et al. Cancer Nanotechnology*   (2024) 15:62

Page 18 of 20

Conclusion

This study highlights the promising potential of CeO$_2$:Ag/GO nanoparticles (NPs) as a novel therapeutic approach for colorectal cancer (CRC). The synthesized NPs demonstrated notable cytotoxicity against CRC cells while exhibiting minimal toxicity to normal cells, making them a compelling option for targeted cancer therapy. The presence of graphene oxide (GO) enhanced the anticancer efficacy of the CeO$_2$:Ag NPs, as evidenced by improved cell viability assays and significant modulation of gene expression related to cancer progression and apoptosis pathways. Specifically, CeO$_2$:Ag/GO NPs downregulated key cancer-related genes and upregulated pro-apoptotic genes, indicating their role in disrupting tumor growth mechanisms. While the results are encouraging, further research is needed to delve deeper into the precise molecular mechanisms and pathways affected by these NPs. Additionally, exploring the potential combination of CeO$_2$:Ag/GO NPs with conventional therapies, such as chemotherapy or radiation, could enhance treatment outcomes. These findings lay the groundwork for future investigations and the development of CeO$_2$:Ag/GO-based therapeutics for more effective CRC management.

Declarations

Ethics approval and consent to participate
Not applicable.

Consent for publication
Not applicable.

Competing interests
The authors declare no competing interests.

Author details
[1]Department of Physiology, School of Medicine, Tehran University of Medical Sciences, Tehran, Iran. [2]Department of Laboratory Medicine, School of Allied Medical Sciences, Kashan University of Medical Sciences, Kashan, Iran. [3]Research Center for Biochemistry and Nutrition in Metabolic Diseases, Institute for Basic Sciences, Kashan University of Medical Sciences, Kashan, Iran. [4]Anatomical Sciences Research Center, Institute for Basic Sciences, Kashan University of Medical Sciences, Kashan, Iran. [5]Biotechnology Research Center, Pharmaceutical Technology Institute, Mashhad University of Medical Sciences, Mashhad, Iran. [6]School of Pharmacy, Mashhad University of Medical Sciences, Mashhad, Iran. [7]Electrophysiology Research Center, Neuroscience Institute, Tehran University of Medical Sciences, Tehran, Iran. [8]Department of Chemical Engineering, Amirkabir University of Technology (Tehran Polytechnic), Tehran, Iran. [9]Institute of Nanoscience and Nanotechnology, University of Kashan, Kashan, Iran. [10]Department of Internal Medicine, School of Medicine, Firoozgar Hospital, Iran University of Medical Sciences, Tehran, Iran. [11]Endocrine Research Center, Institute of Endocrinology and Metabolism, Iran University of Medical Sciences (IUMS), Tehran, Iran.

References

Albasri AM, Elkablawy MA, Ansari IA, Alhujaily AS (2019) Prognostic significance of Cyclin D1 over-expression in colorectal cancer: an experience from Madinah, Saudi Arabia. Asian Pac J Cancer Prev APJCP 20(8):2471

Bray F, Laversanne M, Weiderpass E, Soerjomataram I (2021) The ever-increasing importance of cancer as a leading cause of premature death worldwide. Cancer 127(16):3029–3030

Burnett-Hartman AN, Lee JK, Demb J, Gupta S (2021) An update on the epidemiology, molecular characterization, diagnosis, and screening strategies for early-onset colorectal cancer. Gastroenterology 160(4):1041–1049

Casals E, Zeng M, Parra-Robert M, Fernández-Varo G, Morales-Ruiz M, Jimenez W et al (2020) Cerium oxide nanoparticles: advances in biodistribution, toxicity, and preclinical exploration. Small 16(20):1907322

Chen Y, Yang T, Chen S, Qi S, Zhang Z, Xu Y (2020) Silver nanoparticles regulate autophagy through lysosome injury and cell hypoxia in prostate cancer cells. J Biochem Mol Toxicol 34(5):e22474

Clevers H, Nusse R (2012) Wnt/β-catenin signaling and disease. Cell 149(6):1192–1205

Clevers H, Loh KM, Nusse R (2014) An integral program for tissue renewal and regeneration: Wnt signaling and stem cell control. Science 346(6205):1248012

Danhier F, Feron O, Préat V (2010) To exploit the tumor microenvironment: Passive and active tumor targeting of nanocarriers for anti-cancer drug delivery. J Control Release 148(2):135–146

Datta A, Mishra S, Manna K, Saha KD, Mukherjee S, Roy S (2020) Pro-oxidant therapeutic activities of cerium oxide nanoparticles in colorectal carcinoma cells. ACS Omega 5(17):9714–9723

De la Roche M, Worm J, Bienz M (2008) The function of BCL9 in Wnt/β-catenin signaling and colorectal cancer cells. BMC Cancer 8:1–13

De Marzi L, Monaco A, De Lapuente J, Ramos D, Borras M, Di Gioacchino M et al (2013) Cytotoxicity and genotoxicity of ceria nanoparticles on different cell lines in vitro. Int J Mol Sci 14(2):3065–3077

Dezfuli AS, Ganjali MR, Naderi HR, Norouzi P (2015) A high performance supercapacitor based on a ceria/graphene nanocomposite synthesized by a facile sonochemical method. RSC Adv 5(57):46050–46058

Duan Y, Pang H, Zhang Y, Chen J, Wang T (2016) Morphology-controlled synthesis and microwave absorption properties of β-MnO2 microncube with rectangular pyramid. Mater Charact 112:206–212

Ganjouzadeh F, Khorrami S, Gharbi S (2022) Controlled cytotoxicity of Ag-GO nanocomposite biosynthesized using black peel pomegranate extract against MCF-7 cell line. J Drug Deliv Sci Technol 71:103340

Govender R, Phulukdaree A, Gengan RM, Anand K, Chuturgoon AA (2013) Silver nanoparticles of Albizia adianthifolia: the induction of apoptosis in human lung carcinoma cell line. J Nanobiotechnol 11:1–9

Habiba K, Aziz K, Sanders K, Santiago CM, Mahadevan LSK, Makarov V et al (2019) enhancing colorectal cancer radiation therapy efficacy using silver nanoprisms decorated with graphene as radiosensitizers. Sci Rep 9(1):17120

Hadrup N, Loeschner K, Mortensen A, Sharma AK, Qvortrup K, Larsen EH, Lam HR (2012) The similar neurotoxic effects of nanoparticulate and ionic silver in vivo and in vitro. Neurotoxicology 33(3):416–423

Hansora D, Shimpi N, Mishra S (2015) Graphite to graphene via graphene oxide: an overview on synthesis, properties, and applications. Jom 67:2855–2868

Hossen S, Hossain MK, Basher MK, Mia MNH, Rahman MT, Uddin MJ (2019) Smart nanocarrier-based drug delivery systems for cancer therapy and toxicity studies: a review. J Adv Res 15:1–18

Hummers WS, Offeman RE (1958) Preparation of graphitic oxide. J Am Chem Soc 80(6):1339

Inbaraj BS, Chen B-H (2020) An overview on recent in vivo biological application of cerium oxide nanoparticles. Asian J Pharm Sci 15(5):558–575

Jafarinejad-Farsangi S, Hashemi MS, Rouholamini SEY, Gharbi S, Ansari-Asl Z, Jafari E et al (2021) Curcumin loaded on graphene nanosheets induced cell death in mammospheres from MCF-7 and primary breast tumor cells. Biomed Mater 16(4):045040

Jeevanandam J, Kiew SF, Boakye-Ansah S, Lau SY, Barhoum A, Danquah MK, Rodrigues J (2022) Green approaches for the synthesis of metal and metal oxide nanoparticles using microbial and plant extracts. Nanoscale 14(7):2534–2571

Jeyaraj M, Sathishkumar G, Sivanandhan G, MubarakAli D, Rajesh M, Arun R et al (2013) Biogenic silver nanoparticles for cancer treatment: an experimental report. Colloids Surf, B 106:86–92

Ji Y, Lv J, Sun D, Huang Y (2022) Therapeutic strategies targeting Wnt/β-catenin signaling for colorectal cancer. Int J Mol Med 49(1):1–17

Jung Y-S, Jun S, Lee SH, Sharma A, Park J-I (2015) Wnt2 complements Wnt/β-catenin signaling in colorectal cancer. Oncotarget 6(35):37257

Kasprzak A (2020) Angiogenesis-related functions of Wnt signaling in colorectal carcinogenesis. Cancers 12(12):3601

Khan I, Saeed K, Khan I (2019) Nanoparticles: properties, applications and toxicities. Arab J Chem 12(7):908–931

Kovács D, Igaz N, Gopisetty MK, Kiricsi M (2022) Cancer therapy by silver nanoparticles: fiction or reality? Int J Mol Sci 23(2):839

Kumar E, Selvarajan P, Balasubramanian K (2010) Preparation and studies of cerium dioxide (CeO2) nanoparticles by microwave-assisted solution method. Recent Res Sci Technol 2(4):37

Li L, Sun J, Li X, Zhang Y, Wang Z, Wang C et al (2012) Controllable synthesis of monodispersed silver nanoparticles as standards for quantitative assessment of their cytotoxicity. Biomaterials 33(6):1714–1721

Liao K-H, Lin Y-S, Macosko CW, Haynes CL (2011) Cytotoxicity of graphene oxide and graphene in human erythrocytes and skin fibroblasts. ACS Appl Mater Interfaces 3(7):2607–2615

Lin W, Huang YW, Zhou XD, Ma Y (2006) Toxicity of cerium oxide nanoparticles in human lung cancer cells. Int J Toxicol 25(6):451–457

Maeda H, Nakamura H, Fang J (2013) The EPR effect for macromolecular drug delivery to solid tumors: Improvement of tumor uptake, lowering of systemic toxicity, and distinct tumor imaging in vivo. Adv Drug Deliv Rev 65(1):71–79

Mata R, Nakkala JR, Sadras SR (2015) Biogenic silver nanoparticles from Abutilon indicum: their antioxidant, antibacterial and cytotoxic effects in vitro. Colloids Surf, B 128:276–286

Mittal S, Pandey AK (2018) Corrigendum to "cerium oxide nanoparticles induced toxicity in human lung cells: role of ROS mediated DNA damage and apoptosis." Biomed Res Int 2018:6349540

Tamtaji *et al. Cancer Nanotechnology*   *(2024) 15:62*

Page 20 of 20

Nithya P, Sundrarajan M (2020) Ionic liquid functionalized biogenic synthesis of Ag–Au bimetal doped CeO2 nanoparticles from Justicia adhatoda for pharmaceutical applications: antibacterial and anti-cancer activities. J Photochem Photobiol, B 202:111706

Nowak-Sliwinska P, Scapozza L, Altaba AR (2019) Drug repurposing in oncology: compounds, pathways, phenotypes and computational approaches for colorectal cancer. Biochimica Et Biophysica Acta (BBA) Rev Cancer 1871:434–454

Raj S, Khurana S, Choudhari R, Kesari KK, Kamal MA, Garg N et al (2021) Specific targeting cancer cells with nanoparticles and drug delivery in cancer therapy. Semin Cancer Biol. https://doi.org/10.1016/j.semcancer.2019.11.002

Sharma G, Prema D, Venkataprasanna K, Prakash J, Sahabuddin S, Venkatasubbu GD (2020) Photo induced antibacterial activity of CeO2/GO against wound pathogens. Arab J Chem 13(11):7680–7694

Shen J, Dong J, Shao F, Zhao J, Gong L, Wang H et al (2022) Graphene oxide induces autophagy and apoptosis via the ROS-dependent AMPK/mTOR/ULK-1 pathway in colorectal cancer cells. Nanomedicine (Lond) 17(9):591–605

Siegel RL, Miller KD, Goding Sauer A, Fedewa SA, Butterly LF, Anderson JC et al (2020) Colorectal cancer statistics, 2020. CA Cancer J Clin 70(3):145–164

Simard JC, Durocher I, Girard D (2016) Silver nanoparticles induce irremediable endoplasmic reticulum stress leading to unfolded protein response dependent apoptosis in breast cancer cells. Apoptosis 21(11):1279–1290

Singh M, Gupta P, Baronia R, Singh P, Karuppiah S, Shankar R et al (2018) In vitro cytotoxicity of GO–DOx on FaDu squamous carcinoma cell lines. Int J Nanomed 13(sup1):107–111

Spitalsky Z, Danko M, Mosnacek J (2011) Preparation of functionalized graphene sheets. Curr Org Chem 15(8):1133–1150

Sun T, Zhang YS, Pang B, Hyun DC, Yang M, Xia Y (2021) Engineered nanoparticles for drug delivery in cancer therapy. In: Voliani V (ed) Nanomaterials and neoplasms. Jenny Stanford Publishing, Singapore, pp 31–142

Sun B, Chen W, Zhang H, Feng T, Xing W, Elmarakbi A, Fu Y-Q (2023) CeO2-decorated reduced graphene oxide for lubricative, anticorrosive and photocatalytic purposes. Mater Chem Phys 308:128255

Sung H, Ferlay J, Siegel RL, Laversanne M, Soerjomataram I, Jemal A, Bray F (2021) Global cancer statistics 2020: GLOBOCAN estimates of incidence and mortality worldwide for 36 cancers in 185 countries. CA Cancer J Clin 71(3):209–249

Umar S (2014) Enteric pathogens and cellular transformation: bridging the gaps. Oncotarget 5(16):6573

Utsunomiya T, Doki Y, Takemoto H, Shiozaki H, Yano M, Sekimoto M et al (2001) Correlation of beta-catenin and cyclin D1 expression in colon cancers. Oncology 61(3):226–233

Valenzuela-Salas LM, Girón-Vázquez NG, García-Ramos JC, Torres-Bugarín O, Gómez C, Pestryakov A et al (2019) Antiproliferative and antitumour effect of nongenotoxic silver nanoparticles on melanoma models. Oxid Med Cell Longev. https://doi.org/10.1155/2019/4528241

Wang P, Meng F, Gao C, Xie W, Wang J, Li A (2018) Structural, morphological and optical characteristics of fusiform Co-doped CeO 2 via a facile hydrothermal method. J Mater Sci Mater Electron 29:11482–11488

Wang J, Li Y, Nie G (2021) Multifunctional biomolecule nanostructures for cancer therapy. Nat Rev Mater 6(9):766–783

Wason MS, Lu H, Yu L, Lahiri SK, Mukherjee D, Shen C et al (2018) Cerium oxide nanoparticles sensitize pancreatic cancer to radiation therapy through oxidative activation of the JNK apoptotic pathway. Cancers 10(9):303

Wu Y, Yang X, Chen Z, Tian L, Jiang G, Chen F et al (2019) m6A-induced lncRNA RP11 triggers the dissemination of colorectal cancer cells via upregulation of Zeb1. Mol Cancer 18(1):1–16

Yildiz G, Bolton-Warberg M, Awaja F (2021) Graphene and graphene oxide for bio-sensing: general properties and the effects of graphene ripples. Acta Biomater 131:62–79

Zhang Z, Kleinstreuer C, Donohue JF, Kim C (2005) Comparison of micro-and nano-size particle depositions in a human upper airway model. J Aerosol Sci 36(2):211–233

Zhang X-F, Choi Y-J, Han JW, Kim E, Park JH, Gurunathan S, Kim J-H (2015) Differential nanoreprotoxicity of silver nanoparticles in male somatic cells and spermatogonial stem cells. Int J Nanomed. https://doi.org/10.2147/IJN.S76062

Publisher's Note

Springer Nature remains neutral with regard to jurisdictional claims in published maps and institutional affiliations.